
There Was Never a Bottleneck in Concept Bottleneck Models

Antonio Almudévar
 ViVoLab, I3A
 University of Zaragoza
 almudevar@unizar.es

José Miguel Hernández-Lobato
 Machine Learning Group
 University of Cambridge
 jmh233@cam.ac.uk

Alfonso Ortega
 ViVoLab, I3A
 University of Zaragoza
 ortega@unizar.es

Abstract

Deep learning representations are often difficult to interpret, which can hinder their deployment in sensitive applications. Concept Bottleneck Models (CBMs) have emerged as a promising approach to mitigate this issue by learning representations that support target task performance while ensuring that each component predicts a concrete concept from a predefined set. In this work, we argue that CBMs do not impose a true bottleneck: the fact that a component can predict a concept does not guarantee that it encodes only information about that concept. This shortcoming raises concerns regarding interpretability and the validity of intervention procedures. To overcome this limitation, we propose Minimal Concept Bottleneck Models (MCBMs), which incorporate an Information Bottleneck (IB) objective to constrain each representation component to retain only the information relevant to its corresponding concept. This IB is implemented via a variational regularization term added to the training loss. As a result, MCBMs yield more interpretable representations, support principled concept-level interventions, and remain consistent with probability-theoretic foundations.

1 Introduction

Most machine learning models operate by learning data representations—compressed versions of the input that retain the essential information needed to solve a given task [1]. However, these representations often encode information in ways that are not easily interpretable by humans. This lack of interpretability becomes especially problematic in sensitive domains such as healthcare [2–4], finance [5, 6], and autonomous driving [7, 8]. To address this issue, *Concept Bottleneck Models* (CBMs) have been proposed, which enforce representations to be defined in terms of a set of human-understandable concepts [9].

Formally, given a task \mathbf{y} and a set of concepts $\mathbf{c} = \{c_j\}_{j=1}^m$, Vanilla Models (VMs) are trained with a single objective: their representations \mathbf{z} should capture the information necessary to predict \mathbf{y} accurately. CBMs extend this framework by adding a second objective: each concept c_j must be recoverable from a designated component $z_j \in \mathbf{z}$. By enforcing this additional constraint, CBMs are claimed to offer: (i) improved interpretability of the representation space, and (ii) the ability to intervene on specific concepts by modifying z_j and propagating these changes to the predictions.

However, CBMs are prone to a phenomenon known as *information leakage* [10, 11], where the representation \mathbf{z} encodes input information that cannot be attributed to the predefined concepts \mathbf{c} . We refer to this additional information as *nuisances* \mathbf{n} . Information leakage raises two main concerns: (i) it undermines interpretability, since z_j cannot be fully explained by its corresponding concept c_j ; and (ii) it compromises the validity of interventions—modifying z_j may alter not only the associated concept c_j , but also other unintended information encoded in z_j .

We argue that *information leakage* stems from a fundamental limitation in the current formulation of CBMs: the absence of an explicit Information Bottleneck (IB) [12] that actively constrains z_j

to exclude information unrelated to c_j . While the second objective in CBMs encourages each z_j to retain c_j in its entirety, it does not enforce that z_j captures only information about c_j . In the worst-case scenario, z_j could encode the entire input x and still satisfy this objective.

To address this issue, we propose *Minimal Concept Bottleneck Models* (MCBMs), which incorporate an IB into each z_j . This ensures that z_j not only retains all the information about its associated concept c_j , but also excludes any information unrelated to

c_j , as summarized in Table 1. The name reflects that z_j is trained to be a *minimal sufficient* statistic of c_j [13, 14], in contrast to traditional CBMs where z_j is optimized to be merely a *sufficient* statistic of c_j . As illustrated in Figure 1, this design yields disentangled representations that directly address the two shortcomings of CBMs: (i) it improves interpretability, since z_j can be fully explained by its corresponding concept c_j ; and (ii) it enables valid interventions—modifying z_j affects only the associated concept c_j .

In Section 2, we connect the data generative process to MCBMs through information-theoretic quantities, showing that the IB can be implemented via a variational loss. In Section 3, we review alternative approaches to address information leakage. In Section 4, we present experiments demonstrating that MCBMs enforce a true bottleneck, thereby enhancing interpretability and intervenability compared to existing alternatives. Finally, in Section 5, we show that the assumptions made in CBMs to enable interventions are theoretically flawed.

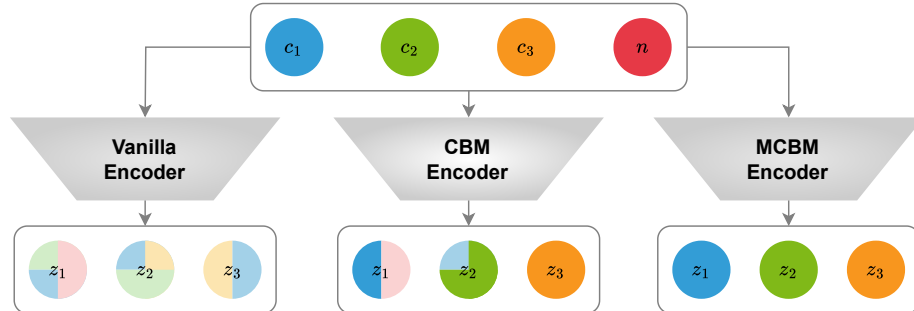


Figure 1: In Vanilla Models, concepts and nuisances may be arbitrarily entangled in the representation, and a variable z_j may capture only part of a concept (depicted as paler colors). In CBMs, each z_j encodes all information about its corresponding concept c_j , but may also capture some information about nuisances (e.g., z_1) or other concepts (e.g., z_2). In contrast, MCBMs enforce that each representation variable z_j encodes all—and only—the information about its corresponding concept.

2 From Data Generative Process to MCBMs

2.1 Data Generative Process

For this scenario, we consider inputs $x \in \mathcal{X}$, targets $y \in \mathcal{Y}$, concepts $c = \{c_j\}_{j=1}^m \in \mathcal{C}$ and nuisances $n \in \mathcal{N}$, such that $p(x, y, c, n) = p(x|c, n)p(y|x)$, i.e., the inputs x are described by the concepts c and the nuisances n , and the targets y are fully described by the input x . The only difference between c and n is that the former are observed, while the latter are not or, in other words, labels on c are provided to us. We assume access to a training set $\{\mathbf{x}^{(i)}, \mathbf{y}^{(i)}, \mathbf{c}^{(i)}\}_{i=1}^N$, which defines the empirical distribution $p(x, y, c) = \sum_{i=1}^N \delta(\mathbf{x} - \mathbf{x}^{(i)}) \delta(\mathbf{y} - \mathbf{y}^{(i)}) \delta(\mathbf{c} - \mathbf{c}^{(i)})$. The graphical model corresponding to this generative process is shown in Figure 2a for the case of two concepts.

2.2 Vanilla Models

In machine learning, the most commonly studied problem is that of predicting y from x , which serves as a foundation for more specialized tasks. We refer to models trained to address this problem as *Vanilla Models* (VMs). These models typically operate by first extracting an intermediate representation $z \in \mathcal{Z}$ from the input x via an *encoder* $p_\theta(z | x)$. Subsequently, a prediction $\hat{y} \in \mathcal{Y}$ is

produced from \mathbf{z} using a *task head* $q_\phi(\hat{\mathbf{y}} \mid \mathbf{z})$. Since \mathbf{z} is intended to facilitate accurate prediction of \mathbf{y} , the mutual information between \mathbf{z} and \mathbf{y} , denoted $I(Z; Y)$, should be maximized. In Appendix B.1, we formally show that:

$$\max_{Z} I(Z; Y) = \max_{\theta, \phi} \mathbb{E}_{p(\mathbf{x}, \mathbf{y})} [\mathbb{E}_{p_\theta(\mathbf{z} \mid \mathbf{x})} [\log q_\phi(\hat{\mathbf{y}} \mid \mathbf{z})]] \quad (1)$$

Figure 2b shows the graphical model of a Vanilla Model with a two-dimensional representation \mathbf{z} . Black edges represent the encoder $p_\theta(\mathbf{z} \mid \mathbf{x})$, while green edges indicate the task head $q_\phi(\hat{\mathbf{y}} \mid \mathbf{z})$. The *encoder* is typically chosen to be deterministic, i.e., $p_\theta(\mathbf{z} \mid \mathbf{x}) = \delta(\mathbf{z} - f_\theta(\mathbf{x}))$. However, for tractability reasons (see Section 2.4), we adopt a stochastic formulation where $p_\theta(\mathbf{z} \mid \mathbf{x}) = \mathcal{N}(\mathbf{z}; f_\theta(\mathbf{x}), \sigma_x^2 I)$, as summarized in Table 2. The choice of *task head* $q_\phi(\hat{\mathbf{y}} \mid \mathbf{z})$ depends on the structure of the output space \mathcal{Y} , also detailed in Table 2. The objective in Equation 1 corresponds to minimizing the cross-entropy loss when \mathbf{y} is binary or multiclass, and to minimizing the mean squared error between \mathbf{y} and $g_\phi^y(\mathbf{z})$ when \mathbf{y} is continuous.

2.3 Concept Bottleneck Models

Vanilla Models generally lack interpretability with respect to the known concepts \mathbf{c} , as the encoder f_θ is often opaque and difficult to analyze. Moreover, these models tend to entangle the concepts in such a way that it becomes intractable to determine how individual concepts influence specific components of the latent representation \mathbf{z} , and consequently the predictions $\hat{\mathbf{y}}$. *Concept Bottleneck Models* (CBMs) have been introduced to address this limitation. In a CBM, each concept c_j is predicted from a dedicated latent representation z_j via a *concept head* $q(\hat{c}_j \mid z_j)$. Consequently, z_j must encode all information about c_j —that is, z_j must be a *sufficient* representation for c_j . This requirement can be formalized as maximizing the mutual information $I(Z_j; C_j)$, for which the following identity—proved in Appendix B.2—is employed:

$$\max_{Z_j} I(Z_j; C_j) = \max_{\theta, \phi} \mathbb{E}_{p(\mathbf{x}, c_j)} [\mathbb{E}_{p_\theta(z_j \mid \mathbf{x})} [\log q_\phi(\hat{c}_j \mid z_j)]] \quad (2)$$

As illustrated in Figure 2c, CBMs extend Vanilla Models by incorporating a concept head $q(\hat{c}_j \mid z_j)$, depicted with blue arrows. These models jointly optimize the objectives in Equations 1 and 2. As detailed in Table 2, the form of the concept head $q_\phi(\hat{c}_j \mid z_j)$ depends on the nature of the concept space \mathcal{C} . The objective in Equation 2 corresponds to minimizing the cross-entropy loss when c_j is binary or multiclass, and the mean squared error between c_j and $g_\phi^c(z_j)$ when c_j is continuous.

How are Interventions Performed in CBMs? As explained in Section 1, a key advantage often attributed to CBMs is their ability to support concept-level interventions. Suppose we aim to estimate $p(\hat{\mathbf{y}} \mid c_j = \alpha, \mathbf{x})$. In CBMs, this intervention is performed through the latent representation z_j :

$$p(\hat{\mathbf{y}} \mid c_j = \alpha, \mathbf{x}) = \iint p(\hat{\mathbf{y}} \mid z_j, \mathbf{z}_{\setminus j}) p(z_j \mid c_j = \alpha) p(\mathbf{z}_{\setminus j} \mid \mathbf{x}) dz_j d\mathbf{z}_{\setminus j} \quad (3)$$

However, the conditional distribution $p(z_j \mid c_j)$ is not defined—there is no directed path from c_j to z_j in Figure 2c. Intuitively, because z_j may encode information about \mathbf{x} beyond c_j , it cannot be fully determined by c_j alone. This raises a key question: *how can interventions be performed in CBMs if $p(z_j \mid c_j)$ is unknown?* To make interventions feasible, CBMs typically impose two constraints:

- (i) Concepts $c_j \in \mathbf{c}$, are assumed to be binary. If a concept is originally multiclass with k categories, it is converted into k binary concepts (One-vs-Rest [15]).
- (ii) The *concept head* is defined as $q_\phi(c_j \mid z_j) = \sigma(z_j)$, where σ denotes the sigmoid function.

Since σ is invertible, this setup permits defining $p(z_j \mid c_j) \approx \sigma^{-1}(c_j)$. However, this is ill-defined at the binary extremes, as $\sigma^{-1}(1) = -\sigma^{-1}(0) = \infty$. To address this, in practice, $p(z_j \mid c_j = 0)$ and $p(z_j \mid c_j = 1)$ are set as the 5th and 95th percentiles of the empirical distribution of z_j , respectively [9]. This workaround, however, introduces two crucial issues discussed in Section 5.

Table 2: Distributions considered in this work. f_θ is typically modeled by a large neural network while g_ϕ^y , g_ϕ^c and g_ϕ^z by simpler neural networks. We consider \mathbf{z} to be always continuous.

	$p_\theta(z \mid \mathbf{x})$	$q_\phi(\hat{\mathbf{y}} \mid \mathbf{z})$	$q_\phi(\hat{c}_j \mid z_j)$	$q_\phi(\hat{z}_j \mid c_j)$
Binary	-	Bernoulli $\left(g_\phi^y(z) \right)$	Bernoulli $\left(g_\phi^c(z_j) \right)$	-
Multiclass	-	Categoric $\left(g_\phi^y(z) \right)$	Categoric $\left(g_\phi^c(z_j) \right)$	-
Continuous	$\mathcal{N}(f_\theta(\mathbf{x}), \sigma_x^2 I)$	$\mathcal{N}\left(g_\phi^y(z), \sigma_y^2 I\right)$	$\mathcal{N}\left(g_\phi^c(z_j), \sigma_c^2 I\right)$	$\mathcal{N}\left(g_\phi^z(c_j), \sigma_z^2 I\right)$

2.4 Minimal Concept Bottleneck Models

As discussed in Section 1, CBMs lack an explicit mechanism for enforcing a bottleneck, which often undermines their intended advantages. To address this limitation, we introduce *Minimal Concept Bottleneck Models* (MCBMs), which explicitly impose an *Information Bottleneck*. This ensures that each z_j retains all information about its associated concept c_j , while excluding information unrelated to c_j . In other words, z_j becomes a *minimal sufficient* representation of c_j . To achieve this, we introduce a *representation head* $q_\phi(\hat{z}_j | c_j)$ that predicts z_j from c_j . This encourages z_j to discard information unrelated to c_j , as doing so improves the predictive accuracy of $q_\phi(\hat{z}_j | c_j)$. Formally, this objective corresponds to minimizing the conditional mutual information $I(Z_j; \hat{X} | C_j)$. We note that if z_j is a representation of x , then the following propositions are equivalent: (i) $I(Z_j; X | C_j) = 0$, (ii) the Markov Chain $X \leftrightarrow C_j \leftrightarrow Z_j$ is satisfied and (iii) $p(z_j | c_j) = p(z_j | x)$. To minimize $I(Z_j; X | C_j)$, we leverage the following identity, which is proven in Appendix B.3:

$$\min_{Z_j} I(Z_j; X | C_j) = \min_{\theta, \phi} \mathbb{E}_{p(x, c_j)} [D_{KL}(p_\theta(z_j | x) || q_\phi(\hat{z}_j | c_j))] \quad (4)$$

Figure 2d illustrates how MCBMs extend CBMs by introducing the representation head $q(\hat{z}_j | c_j)$, depicted with red arrows. These models are trained to jointly optimize the objectives given in Equations 1, 2, and 4. Although the KL Divergence in Equation 4 does not admit a closed-form solution in general, we show in Appendix B.4 that, under the distributional assumptions listed in Table 2, it reduces to the mean squared error between $f_\theta(x)$ and $g_\phi^z(c_j)$.

How are Interventions Performed in MCBMs? In contrast to CBMs, MCBMs explicitly constrain z_j to contain only information about c_j . As a result, modifying z_j corresponds to intervening solely on c_j . This is reflected in Figure 2d, where MCBMs introduce a directed path from c_j to z_j through the intermediate variable \hat{z}_j . This structure permits the computation of:

$$p(z_j | c_j) = \int p(z_j | \hat{z}_j) q_\phi(\hat{z}_j | c_j) d\hat{z}_j \quad (5)$$

which simplifies to $p(z_j | c_j) = q_\phi(z_j | c_j)$ when $p(z_j | \hat{z}_j) = \delta(z_j - \hat{z}_j)$, i.e., once the objective in Equation 4 is optimized and z_j encodes exclusively c_j . As shown in Table 2, we define the encoder distribution as $q_\phi(z_j | c_j) = \mathcal{N}(g_\phi^z(c_j), \sigma_z^2 I)$, where mean function $g_\phi^z(c_j)$ is chosen according to the following rules:

- (i) For binary concepts, $g_\phi^z(c_j) = \lambda$ if $c_j = 1$, and $g_\phi^z(c_j) = -\lambda$ otherwise.
- (ii) For categorical concepts, $g_\phi^z(c_j) = \lambda \cdot \text{one_hot}(c_j)$. This mirrors the *Prototypical Learning* [16] approach where class-dependent prototypes $\{g_\phi^z(c_j)\}_{j=1}^m$ are fixed.
- (iii) For continuous concepts, $g_\phi^z(c_j) = \lambda \cdot c_j$.

Here, λ is a scaling constant that controls the norm of the latent representation, fixed to $\lambda = 3$ in all experiments. Regarding the variance term, we set: (i) $\sigma_x = 0$ in the case of CBMs to obtain a deterministic encoder in line with their original formulation, and (ii) $\sigma_x = \sigma_z = 1$ for MCBMs.

Practical Considerations for Optimizing MCBMs To optimize MCBMs, we combine the three previously introduced objectives, incorporating two key considerations. First, we approximate the expectations over $p(x, y)$ and $p(x, c_j)$ using the empirical data distribution, replacing integrals with summations over the dataset. Second, to enable gradient-based optimization through the stochastic encoder, we apply the reparameterization trick [17]: $\mathbb{E}_{p_\theta(z|x)} [\log q_\phi(y|z)] \approx \sum_i \log q_\phi(y|f'_\theta(x, \epsilon^{(i)}))$ and $E_{p_\theta(z_j|x)} [\log q_\phi(\hat{c}_j|z_j)] \approx \sum_i \log q_\phi(\hat{c}_j|f'_{\theta,j}(x, \epsilon^{(i)}))$, where $f'_\theta(x, \epsilon) = f_\theta(x) + \sigma_x^2 I \epsilon$ (due to the choice of $p_\theta(z|x)$ in Table 2), $\epsilon \sim \mathcal{N}(0, I)$ and $f'_{\theta,j}(x, \epsilon)$ corresponds to the element j of $f'_\theta(x, \epsilon)$. Combining the considerations above yields the final objective for training MCBMs, as shown in Equation 6, where β and γ are hyperparameters. The first term corresponds to the objective used in Vanilla Models, the second term is introduced in CBMs, and the third is specific to MCBMs. Detailed training algorithms for the various cases listed in Table 2 are provided in Appendix C.

$$\begin{aligned} \max_{\theta, \phi} \sum_{k=1}^N \sum_i \log q_\phi(\hat{y}|f'_\theta(x^{(k)}, \epsilon^{(i)})) + \beta \sum_{j=1}^n \log q_\phi(\hat{c}_j|f'_{\theta,j}(x^{(k)}, \epsilon^{(i)})) \\ - \gamma \sum_{j=1}^n D_{KL}(p_\theta(z_j | x^{(k)}) || q_\phi(\hat{z}_j | c_j^{(k)})) \end{aligned} \quad (6)$$

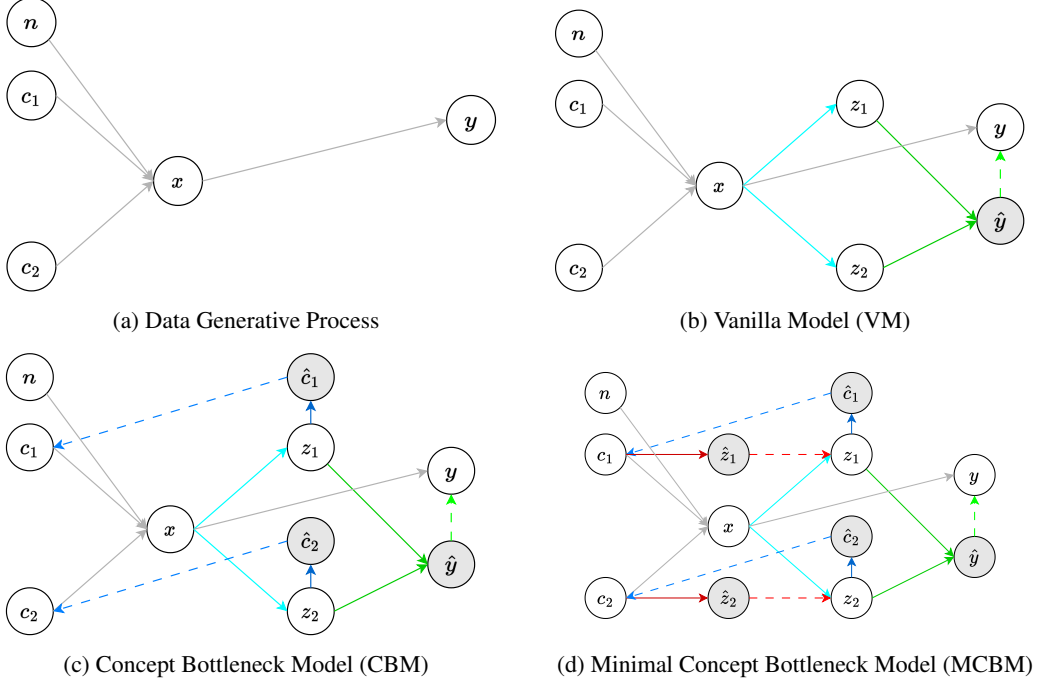


Figure 2: Graphical models of the different systems described for two concepts and two-dimensional representations. We provide in Appendix A the analogous figure for m concepts and m -dimensional representations. Inputs \mathbf{x} are defined by some concepts $\{c_j\}_{j=1}^m$ and nuisances \mathbf{n} ; and targets \mathbf{y} are defined by \mathbf{x} (gray arrows). Vanilla models obtain the representations $\{z_j\}_{j=1}^m$ from \mathbf{x} through the *encoder* $p_\theta(\mathbf{z}|\mathbf{x})$ (cyan arrows) and solve the task $\hat{\mathbf{y}}$ sequentially through the *task head* $q_\phi(\hat{\mathbf{y}}|\mathbf{z})$ (green arrows). Concept Bottleneck Models make a prediction \hat{c}_j of each concept c_j from one representation z_j through the *concept head* $q(\hat{c}_j|z_j)$ (blue arrows). Minimal CBMs make a prediction z_j of each representation z_j from one concept c_j through the *representation head* $q(z_j|c_j)$ (red arrows).

3 Related Work

Information Leakage in Concept Bottleneck Models Information leakage occurs when the learned representation \mathbf{z} encodes information outside the concept set \mathbf{c} , reducing both interpretability and intervenability [10, 11]. This arises when the Markovian assumption fails—i.e., when the target \mathbf{y} is not fully determined by the concept set \mathbf{c} , or equivalently, $p(\mathbf{y}|\mathbf{c}) \neq p(\mathbf{y}|\mathbf{c}, \mathbf{x})$, which is typically the case in real-world scenarios [18]. Concept Embedding Models (CEMs) [19] were proposed to mitigate the accuracy–interpretability trade-off in CBMs. However, this trade-off is fundamentally limited by the chosen concept set, and CEMs may even be less interpretable than standard CBMs, as their more entropic representations tend to amplify information leakage. Recently, this critique has been further formalized: Parisini et al. [20] proposed information-theoretic benchmarks for assessing interpretability and Makonnen et al. [21] introduced new metrics grounded in usable mutual information [22]. Havasi et al. [18] also introduced Hard Concept Bottleneck Models (HCBMs), which predict \mathbf{y} from binarized concept predictions \hat{c}_j rather than from \mathbf{z} (see Appendix D), thereby imposing an ad-hoc Information Bottleneck. Extensions such as Autoregressive CBMs and Stochastic CBMs [18, 23] incorporate dependencies between concepts.

Information Bottleneck in Representation Learning The Information Bottleneck (IB) [12] provides a principled way to balance preserving information about a factor with compressing the representation. In this framework, a representation is *sufficient* if it retains all the information about the variable of interest, and *minimal* if it contains only that information [24–26]. Computation of these quantities is intractable, so variational methods have been developed to derive tractable evidence bounds [27, 28].

4 Experiments

In this section, we present a series of experiments designed to empirically demonstrate that CBMs fail to impose an effective bottleneck, even in simple settings. We also examine the consequences of this limitation. In contrast, we show that MCBMs successfully enforce a bottleneck, thereby mitigating the issues that arise in its absence. Further implementation details—including encoder architectures and training hyperparameters for each experiment—are provided in Appendix E and at https://github.com/antonioalmudevar/minimal_cbm.

4.1 Do CBMs and MCBMs Leak Information?

Some works assume that the task \mathbf{y} is fully defined by the concepts \mathbf{c} . However, it is unrealistic to expect a finite set of human-understandable concepts to completely describe an arbitrarily complex task. In practice, certain nuisances \mathbf{n} that describe the input \mathbf{x} also influence \mathbf{y} . Specifically, we decompose the nuisances as $\mathbf{n} = \{\mathbf{n}_y, \mathbf{n}_{\bar{y}}\}$, where \mathbf{n}_y captures nuisances that, together with the concepts, describe \mathbf{y} , while $\mathbf{n}_{\bar{y}}$ comprises those independent of \mathbf{y} (see Figure 3a). As discussed throughout this work, CBMs provide no incentive to remove information unrelated to the concepts. Moreover, since the objective of most models is to solve \mathbf{y} , they are incentivized to preserve not only \mathbf{c} but also \mathbf{n}_y . While this may improve task performance, it comes at the expense of interpretability and valid interventions. For instance, if $z_j \in \mathbf{z}$ is intended to represent the concept $c_j \in \mathbf{c}$, one might assume that modifying z_j corresponds solely to intervening on c_j . However, if z_j also encodes information about \mathbf{n}_y (or even $\mathbf{n}_{\bar{y}}$ as we show later), then modifying z_j also affects the nuisances, invalidating any causal conclusions. By introducing the Information Bottleneck in Equation 4, we explicitly constrain the model to remove nuisances from z_j , thereby restoring the validity of causal analyses involving c_j . We note, however, that this necessarily reduces task performance: if \mathbf{c} is incomplete and solving \mathbf{y} requires information from \mathbf{n} (i.e., $\mathbf{n}_y \neq \emptyset$), excluding \mathbf{n} from \mathbf{z} will lower predictive performance.

We next examine whether \mathbf{n}_y and $\mathbf{n}_{\bar{y}}$ are present in the representations across different CBM variants and datasets. For this purpose, we define the following task-concept configurations: (i) **MPI3D** [29], where \mathbf{y} is the *object shape*, \mathbf{n}_y the *horizontal axis*, $\mathbf{n}_{\bar{y}}$ the *vertical axis*, and \mathbf{c} the remaining generative factors; (ii) **Shapes3D** [30], where \mathbf{y} is the *shape*, \mathbf{n}_y the *floor color* and *wall color*, $\mathbf{n}_{\bar{y}}$ the *orientation*, and \mathbf{c} the remaining factors; (iii) **CIFAR-10** [31], where \mathbf{y} is the standard classification task, \mathbf{c} consists of 64 of the 143 attributes extracted by Oikarinen et al. [32] using GPT-3 [33], and \mathbf{n}_y the remaining attributes, since all nuisances are correlated with \mathbf{y} ; and (iv) **CUB** [34], where \mathbf{y} is the *bird species*, \mathbf{c} includes concepts from twelve randomly selected attribute groups, and \mathbf{n}_y the attributes from the remaining 20 groups. While MCBMs natively support multiclass concepts, the other baselines in our study are limited to binary concepts. To ensure fairness, factors with k classes are therefore represented as k binary concepts.

Table 3: Average value of URR for task-related nuisances \mathbf{n}_y .

	MPI3D	Shapes3D	CIFAR-10	CUB
Vanilla	35.0 ± 1.9	45.5 ± 6.4	19.8 ± 0.7	3.8 ± 1.0
CBM [9]	28.1 ± 0.5	18.1 ± 2.9	18.5 ± 0.7	3.8 ± 0.8
CEM [19]	43.2 ± 5.2	15.8 ± 3.9	27.2 ± 0.8	3.9 ± 1.1
ARCBM [18]	28.2 ± 1.7	18.4 ± 2.1	18.2 ± 0.6	3.9 ± 0.9
SCBM [23]	24.3 ± 0.4	21.8 ± 1.4	18.3 ± 0.7	3.6 ± 0.8
MCBM (low γ)	10.7 ± 0.1	2.5 ± 0.1	18.0 ± 0.5	3.4 ± 0.9
MCBM (medium γ)	6.7 ± 0.2	0.2 ± 0.3	18.1 ± 0.5	2.8 ± 0.8
MCBM (high γ)	0.0 ± 0.0	0.0 ± 0.0	17.6 ± 0.5	2.4 ± 1.0

Task-related information leakage To measure the presence of a nuisance factor $n_j \in \mathbf{n}_y$ in \mathbf{z} , we estimate $I(N_j; Z | C)$ —the information about n_j contained in \mathbf{z} beyond what is explained by \mathbf{c} . Since this quantity is intractable, we approximate it as $\hat{I}(N_j; Z | C) = \hat{H}(N_j | C) - \hat{H}(N_j | C, Z)$,

where $\hat{H}(N_j \mid C) = -\sum_{k=1}^N \log h_\psi^c(\mathbf{c}^{(k)})$ and $\hat{H}(N_j \mid C, Z) = -\sum_{k=1}^N \log h_\psi^{cz}(\mathbf{c}^{(k)}, \mathbf{z}^{(k)})$. Here, h_ψ^c and h_ψ^{cz} are MLP classifiers trained to predict n_j from \mathbf{c} and (\mathbf{c}, \mathbf{z}) , respectively. In Table 3, we report the average value of $\frac{\hat{I}(N_j; Z|C)}{H(N_j)}$ across all $n_j \in \mathbf{n}_y$, which we call *Uncertainty Reduction Ratio* (URR). From these results, we conclude that: (i) CBMs tend to reduce nuisance information compared to VMs, though not consistently; (ii) CEMs generally preserve the largest amount of nuisance information, often exceeding even VMs; (iii) ARCBMs and HCBMs show no systematic advantage over CBMs in terms of nuisance removal; and (iv) MCBMs provide the strongest reduction of nuisance information, particularly as γ increases, which enforces a stricter bottleneck.

Task-unrelated information leakage Neural networks typically discard input information, as their layers are non-invertible [35, 36]. Moreover, since $\mathbf{n}_{\bar{y}}$ is irrelevant for predicting \mathbf{y} , there is no incentive to retain it in the representation \mathbf{z} . One might therefore expect \mathbf{z} to be free of $\mathbf{n}_{\bar{y}}$. However, prior work has shown that neural representations often preserve information not directly related to the task [24, 37]. To examine this, we analyze whether $\mathbf{n}_{\bar{y}}$ is present in \mathbf{z} for MPI3D and Shapes3D—the only settings where $\mathbf{n}_{\bar{y}}$ is non-empty. Table 4 reports URR values for the nuisance variables in $\mathbf{n}_{\bar{y}}$ in. We find that: (i) as in Table 3, CEMs retain more nuisance information than even VMs; and (ii) MCBMs are the only models that consistently eliminate nuisances across all values of γ , as expected: with no incentive to preserve $\mathbf{n}_{\bar{y}}$ and an explicit penalty for doing so, such information is naturally discarded.

Are concepts removed to a greater extent in MCBMs? One might worry that removing nuisance information could also inadvertently eliminate information about the concepts. To test this, we report concept prediction accuracy for CIFAR-10 and CUB in Table 5 (note that all models reach 100% accuracy on MPI3D and Shapes3D). We can observe that (i) no model consistently outperforms the others—some preserve more concept information in CIFAR-10, while others perform slightly better in CUB; and (ii) increasing γ in MCBMs gradually reduces concept accuracy, as stronger regularization may suppress features correlated with the concepts. These results indicate that MCBMs effectively remove nuisance information while largely preserving concept-relevant content.

How does this affect task performance?

As previously discussed, when \mathbf{n}_y is non-empty, restricting \mathbf{z} to contain only information about \mathbf{c} should reduce performance on \mathbf{y} : if \mathbf{c} alone is insufficient to solve \mathbf{y} , then \mathbf{z} cannot achieve perfect accuracy. In Table 6, we observe the following: (i) CBMs and CEMs reach task accuracy comparable to (or even higher than) VMs, indicating that they also rely on \mathbf{n}_y to predict \mathbf{y} ; (ii) ARCBMs and SCBMs achieve lower task accuracy, as they impose a bottleneck after the representations (see Appendix D); and (iii) MCBMs show decreasing task accuracy as γ increases, reflecting the stricter bottleneck applied to the representations. Importantly, this reduction in task accuracy should not be viewed negatively: since all models achieve similar concept accuracy (see Table 5), it indicates that predictions rely less on nuisance information.

Table 4: Average value of URR for task-unrelated nuisances.

	MPI3D	Shapes3D
Vanilla	11.3 ± 0.1	42.7 ± 9.1
CBM	7.4 ± 1.9	20.6 ± 3.3
CEM	15.5 ± 4.2	40.9 ± 1.8
ARCBM	8.7 ± 1.4	26.6 ± 0.5
SCBM	7.0 ± 0.3	21.7 ± 1.7
MCBM (l γ)	0.0 ± 0.0	0.0 ± 0.0
MCBM (m γ)	0.0 ± 0.0	0.0 ± 0.0
MCBM (h γ)	0.0 ± 0.0	0.0 ± 0.0

Table 5: Average concepts accuracy

	CIFAR-10	CUB
CBM	84.8 ± 0.2	96.3 ± 0.1
CEM	84.8 ± 0.2	96.3 ± 0.1
ARCBM	84.3 ± 0.2	96.2 ± 0.1
SCBM	84.3 ± 0.2	96.5 ± 0.1
MCBM (l γ)	84.9 ± 0.1	96.3 ± 0.2
MCBM (m γ)	84.9 ± 0.2	96.1 ± 0.1
MCBM (h γ)	84.8 ± 0.1	95.8 ± 0.3

Table 6: Task accuracy

	MPI3D	Shapes3D	CIFAR-10	CUB
Vanilla	100.0 ± 0.0	100.0 ± 0.0	72.1 ± 0.6	77.4 ± 0.3
CBM	99.9 ± 0.0	100.0 ± 0.0	73.8 ± 0.1	77.6 ± 0.2
CEM	100.0 ± 0.0	100.0 ± 0.0	73.1 ± 0.3	77.5 ± 0.3
ARCBM	24.2 ± 0.6	29.7 ± 0.4	68.9 ± 0.3	75.5 ± 0.8
SCBM	24.2 ± 0.5	29.7 ± 0.3	62.3 ± 0.0	73.5 ± 0.4
MCBM (l γ)	92.7 ± 1.1	100.0 ± 0.0	72.4 ± 0.5	78.3 ± 0.6
MCBM (m γ)	46.0 ± 0.6	32.2 ± 1.5	70.8 ± 0.2	77.4 ± 0.4
MCBM (h γ)	24.9 ± 0.3	30.1 ± 0.2	70.5 ± 0.6	73.5 ± 1.5

4.2 Do MCBMs Yield More Interpretable Representations?

One of the key properties often attributed to CBMs is that their internal representations align with human-interpretable concepts. While this generally holds, we show that MCBMs yield representations that are even more interpretable. To support this claim, we employ two metrics: (i) *Centered Kernel Alignment* (CKA) [38–40], which measures the similarity between learned representations and concept labels (encoded as one-hot vectors); and (ii) *Disentanglement* [41], which assesses whether each dimension of the representation z_j captures at most one concept c_j . These metrics capture interpretability from complementary perspectives: (i) alignment indicates whether the information is organized in a concept-aware fashion; and (ii) disentanglement reflects the extent to which individual concepts are independently encoded in the representations.

Vanilla	1.87	2.88	18.81	33.53	37.53	39.94	42.56	20.66
CBM	78.69	71.02	27.21	62.06	26.67	15.87	61.47	25.80
CEM	72.43	67.91	26.05	60.87	31.67	37.05	64.66	33.42
ARCBM	83.77	57.58	23.23	65.91	34.72	34.05	51.92	29.99
SCBM	86.83	67.64	22.14	69.72	58.04	32.30	50.98	31.22
MCBM (low γ)	97.80	95.37	41.64	85.53	47.87	39.10	55.84	56.60
MCBM (medium γ)	99.63	99.96	38.69	85.77	77.23	93.60	67.36	61.92
MCBM (high γ)	99.98	99.99	41.21	83.73	85.55	98.76	70.49	57.05
	MPI3D	Shapes3D	CIFAR-10	CUB	MPI3D	Shapes3D	CIFAR-10	CUB

Figure 4: CKA (left) and Disentanglement (right). As shown in Figure 4: (i) CBMs, CEMs, ARCBMs, and HCBMs achieve stronger alignment with concepts than Vanilla Models, yet they do not consistently improve disentanglement; and (ii) MCBMs consistently improve both alignment and disentanglement, particularly as γ increases, reflecting the removal of additional nuisances. These results suggest that explicitly eliminating nuisances leads to more interpretable representations.

4.3 Do MCBMs Enable More Reliable Interventions?

Another key property often attributed to CBMs is their capacity to support interventions. Although standard CBM intervention methods suffer from theoretical limitations (see Section 5), they can still be applied in practice. Accordingly, for CBMs we follow the procedure in Section 2.3, for ARCBMs and SCBMs we use the procedure described in Appendix D, and for MCBMs we apply the method in Section 2.4.

To evaluate intervention reliability across models, we adopt the standardized protocol of Koh et al. [9], which tracks how prediction error changes as the number of intervened concepts increases. Following Shin et al. [42], we intervene on the concepts predicted with the lowest confidence. Results for CIFAR-10 and CUB are shown in Figure 5 (note that interventions have minimal effect on MPI3D and Shapes3D, since—as shown in Table 6—the concepts are not strong predictors of the task). From these results, four main observations emerge: (i) CBMs may even increase error when multiple concepts are intervened—an effect of nuisance information leaking into the representation due to the absence of a proper bottleneck; (ii) ARCBMs and SCBMs mitigate this by applying an Information Bottleneck after the representations, which improves intervention effectiveness while leaving interpretability unchanged (Figure 4); (iii) in MCBMs, intervention gains remain largely invariant to γ , as indicated by the nearly parallel trends across its different values; and (iv) at low and medium γ , MCBMs deliver the strongest intervention performance, especially when fewer than 100% of the concepts are intervened, clearly outperforming ARCBMs and SCBMs.

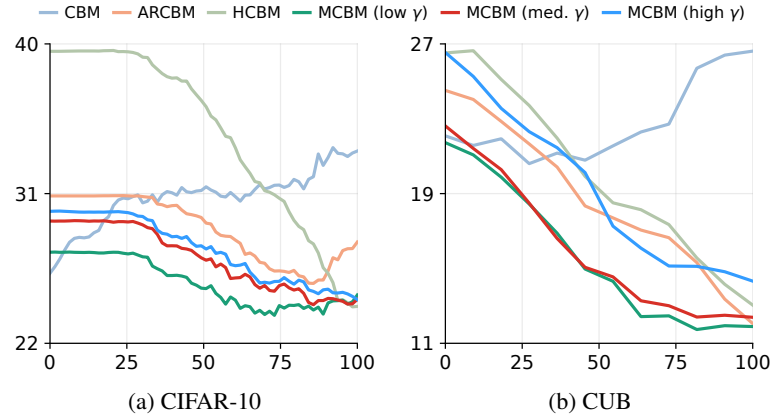


Figure 5: Error (y-axis) versus percentage of concepts intervened (x-axis) across different models.

5 Other Fundamental Theoretical Flaws of CBMs

As briefly discussed in Section 2.3, CBMs—unlike MCBMs—do not provide a principled mechanism to estimate $p(z_j | c_j)$. To enable interventions, two assumptions are typically introduced: (i) multi-class concepts are handled using a One-vs-Rest scheme, and (ii) interventions are implemented via the sigmoid inverse function, i.e., $p(z_j | c_j) \approx \delta(z_j - \sigma^{-1}(c_j))$. These assumptions are not only ad hoc but also theoretically incorrect, as we explain and illustrate with toy experiments below.

One-vs-Rest Limitations One-vs-Rest strategies exhibit several limitations: (i) individual binary classifiers tend to be biased toward the negative class, and (ii) the predicted probabilities across classifiers are typically uncalibrated [43]. To illustrate these issues, we design an experiment where the concepts are defined based on a four-class spiral dataset with imbalanced class distributions. We train: (i) a CBM with One-vs-Rest binarization, and (ii) an MCBM modeling concepts directly as multiclass variables.

The results reveal three major shortcomings of CBMs trained with the One-vs-Rest strategy. First, Figure 6 (left) shows that they overpredict the most frequent class, especially when the true class is rare and spatially close to the dominant. Second, Figure 6 (middle) shows that CBMs produce poorly calibrated predictions, lacking the smooth likelihood transitions observed in MCBMs. Finally, Figure 6 (right) shows that CBMs often assign near-one likelihoods to multiple classes simultaneously, whereas MCBMs confine high secondary likelihoods to regions of overlap, producing more reliable uncertainty estimates. Importantly, these effects may not be captured by standard metrics like accuracy, yet they represent fundamental flaws from a probabilistic perspective.

Sigmoid Inverse Function The intervention procedure $p(z_j | c_j) \approx \delta(z_j - \sigma^{-1}(c_j))$ does not satisfy Bayes’ rule, i.e., $p(z_j | c_j) = \frac{q_\phi(c_j | z_j)p(z_j)}{p(c_j)}$. For example, as illustrated in Figure 7, when the prior $p(z_j)$ is bimodal—a common case for representations arising from two classes— $p(z_j | c_j)$ differs markedly from $\sigma^{-1}(c_j)$. Ignoring the prior therefore not only violates probability theory but also yields poor practical approximations. This issue is difficult to overcome in CBMs, as the prior $p(z_j)$ is unknown and challenging to estimate.

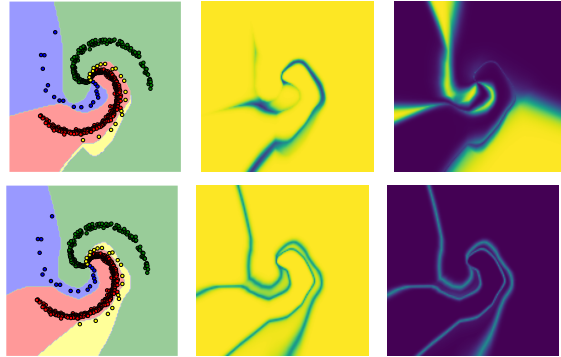


Figure 6: CBM (top) versus MCBM (bottom): class boundaries (left), highest predicted likelihood (middle), and second-highest predicted likelihood (right).

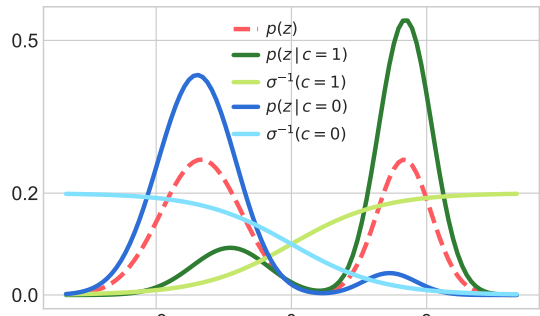


Figure 7: Density (y-axis) vs. z (x-axis)

6 Conclusions

In this paper, we argue that—contrary to common belief—Concept Bottleneck Models (CBMs) do not enforce a true bottleneck: although representations are encouraged to retain concept-related information, they are not constrained to discard nuisance information. This limitation undermines interpretability and provides no theoretical guarantees for intervention procedures. To address this, we propose *Minimal Concept Bottleneck Models* (MCBMs), which introduce an Information Bottleneck in the representation space via an additional loss term derived through variational approximations. Beyond enforcing a proper bottleneck, our formulation ensures that interventions remain consistent with Bayesian principles. Empirically, we show that CBMs and their variants fail to remove non-concept information from the representation, even when irrelevant to the target task. In contrast, MCBMs effectively eliminate such information while preserving concept-relevant content, yielding more interpretable representations and principled interventions. Finally, we highlight fundamental flaws in the intervention process of CBMs, which MCBMs overcome due to their principled design.

Acknowledgments and Disclosure of Funding

This work has received funding from the European Union’s Horizon 2020 research and innovation programme under the Marie Skłodowska-Curie grant agreement No 101007666, MCIN/AEI/10.13039/501100011033 under Grant PID2021-126061OB-C44, and the Government of Aragón (Grant Group T36 23R).

References

- [1] Yoshua Bengio, Aaron Courville, and Pascal Vincent. Representation learning: A review and new perspectives. *IEEE transactions on pattern analysis and machine intelligence*, 35(8):1798–1828, 2013.
- [2] Muhammad Aurangzeb Ahmad, Carly Eckert, and Ankur Teredesai. Interpretable machine learning in healthcare. In *Proceedings of the 2018 ACM international conference on bioinformatics, computational biology, and health informatics*, pages 559–560, 2018.
- [3] Yao Xie, Melody Chen, David Kao, Ge Gao, and Xiang’Anthony’ Chen. Chexplain: enabling physicians to explore and understand data-driven, ai-enabled medical imaging analysis. In *Proceedings of the 2020 CHI Conference on Human Factors in Computing Systems*, pages 1–13, 2020.
- [4] Di Jin, Elena Sergeeva, Wei-Hung Weng, Geeticka Chauhan, and Peter Szolovits. Explainable deep learning in healthcare: A methodological survey from an attribution view. *WIREs Mechanisms of Disease*, 14(3):e1548, 2022.
- [5] Damiano Brigo, Xiaoshan Huang, Andrea Pallavicini, and Haitz Saez de Ocariz Borde. Interpretability in deep learning for finance: a case study for the heston model. *arXiv preprint arXiv:2104.09476*, 2021.
- [6] Shun Liu, Kexin Wu, Chufeng Jiang, Bin Huang, and Danqing Ma. Financial time-series forecasting: Towards synergizing performance and interpretability within a hybrid machine learning approach. *arXiv preprint arXiv:2401.00534*, 2023.
- [7] Jinkyu Kim and John Canny. Interpretable learning for self-driving cars by visualizing causal attention. In *Proceedings of the IEEE international conference on computer vision*, pages 2942–2950, 2017.
- [8] Zhenhua Xu, Yujia Zhang, Enze Xie, Zhen Zhao, Yong Guo, Kwan-Yee K Wong, Zhenguo Li, and Hengshuang Zhao. Drivegpt4: Interpretable end-to-end autonomous driving via large language model. *IEEE Robotics and Automation Letters*, 2024.
- [9] Pang Wei Koh, Thao Nguyen, Yew Siang Tang, Stephen Mussmann, Emma Pierson, Been Kim, and Percy Liang. Concept bottleneck models. In *International conference on machine learning*, pages 5338–5348. PMLR, 2020.
- [10] Andrei Margeiroiu, Matthew Ashman, Umang Bhatt, Yanzhi Chen, Mateja Jamnik, and Adrian Weller. Do concept bottleneck models learn as intended? *arXiv preprint arXiv:2105.04289*, 2021.
- [11] Anita Mahinpei, Justin Clark, Isaac Lage, Finale Doshi-Velez, and Weiwei Pan. Promises and pitfalls of black-box concept learning models. *arXiv preprint arXiv:2106.13314*, 2021.
- [12] Naftali Tishby, Fernando C Pereira, and William Bialek. The information bottleneck method. *arXiv preprint physics/0004057*, 2000.
- [13] Ronald A Fisher. On the mathematical foundations of theoretical statistics. *Philosophical transactions of the Royal Society of London. Series A, containing papers of a mathematical or physical character*, 222 (594-604):309–368, 1922.
- [14] Ronald A Fisher. The logic of inductive inference. *Journal of the royal statistical society*, 98(1):39–82, 1935.
- [15] Ryan Rifkin and Aldebaro Klautau. In defense of one-vs-all classification. *Journal of machine learning research*, 5(Jan):101–141, 2004.
- [16] Jake Snell, Kevin Swersky, and Richard Zemel. Prototypical networks for few-shot learning. *Advances in neural information processing systems*, 30, 2017.
- [17] Diederik P Kingma. Auto-encoding variational bayes. *arXiv preprint arXiv:1312.6114*, 2013.
- [18] Marton Havasi, Sonali Parbhoo, and Finale Doshi-Velez. Addressing leakage in concept bottleneck models. *Advances in Neural Information Processing Systems*, 35:23386–23397, 2022.

[19] Mateo Espinosa Zarlenga, Pietro Barbiero, Gabriele Ciravegna, Giuseppe Marra, Francesco Giannini, Michelangelo Diligenti, Zohreh Shams, Frederic Precioso, Stefano Melacci, Adrian Weller, et al. Concept embedding models: Beyond the accuracy-explainability trade-off. *Advances in Neural Information Processing Systems*, 35:21400–21413, 2022.

[20] Enrico Parisini, Tapabrata Chakraborti, Chris Harbron, Ben D MacArthur, and Christopher RS Banerji. Leakage and interpretability in concept-based models. *arXiv preprint arXiv:2504.14094*, 2025.

[21] Mikael Makonnen, Moritz Vandenhirtz, Sonia Laguna, and Julia E Vogt. Measuring leakage in concept-based methods: An information theoretic approach. *arXiv preprint arXiv:2504.09459*, 2025.

[22] Yilun Xu, Shengjia Zhao, Jiaming Song, Russell Stewart, and Stefano Ermon. A theory of usable information under computational constraints. *arXiv preprint arXiv:2002.10689*, 2020.

[23] Moritz Vandenhirtz, Sonia Laguna, Ričards Marcinkevičs, and Julia Vogt. Stochastic concept bottleneck models. *Advances in Neural Information Processing Systems*, 37:51787–51810, 2024.

[24] Alessandro Achille and Stefano Soatto. Emergence of invariance and disentanglement in deep representations. *Journal of Machine Learning Research*, 19(50):1–34, 2018.

[25] Alessandro Achille and Stefano Soatto. Information dropout: Learning optimal representations through noisy computation. *IEEE transactions on pattern analysis and machine intelligence*, 40(12):2897–2905, 2018.

[26] Ravid Shwartz Ziv and Yann LeCun. To compress or not to compress—self-supervised learning and information theory: A review. *Entropy*, 26(3):252, 2024.

[27] Alexander A Alemi, Ian Fischer, Joshua V Dillon, and Kevin Murphy. Deep variational information bottleneck. *arXiv preprint arXiv:1612.00410*, 2016.

[28] Ian Fischer. The conditional entropy bottleneck. *Entropy*, 22(9):999, 2020.

[29] Muhammad Waleed Gondal, Manuel Wuthrich, Djordje Miladinovic, Francesco Locatello, Martin Breidt, Valentin Volchkov, Joel Akpo, Olivier Bachem, Bernhard Schölkopf, and Stefan Bauer. On the transfer of inductive bias from simulation to the real world: a new disentanglement dataset. *Advances in Neural Information Processing Systems*, 32, 2019.

[30] Hyunjik Kim and Andriy Mnih. Disentangling by factorising. In *International conference on machine learning*, pages 2649–2658. PMLR, 2018.

[31] Alex Krizhevsky, Geoffrey Hinton, et al. Learning multiple layers of features from tiny images. 2009.

[32] Tuomas Oikarinen, Subhro Das, Lam M Nguyen, and Tsui-Wei Weng. Label-free concept bottleneck models. *arXiv preprint arXiv:2304.06129*, 2023.

[33] Tom Brown, Benjamin Mann, Nick Ryder, Melanie Subbiah, Jared D Kaplan, Prafulla Dhariwal, Arvind Neelakantan, Pranav Shyam, Girish Sastry, Amanda Askell, et al. Language models are few-shot learners. *Advances in neural information processing systems*, 33:1877–1901, 2020.

[34] Catherine Wah, Steve Branson, Peter Welinder, Pietro Perona, and Serge Belongie. The caltech-ucsd birds-200-2011 dataset. 2011.

[35] Naftali Tishby and Noga Zaslavsky. Deep learning and the information bottleneck principle. In *2015 ieee information theory workshop (itw)*, pages 1–5. Ieee, 2015.

[36] Michael Tschannen, Josip Djolonga, Paul K Rubenstein, Sylvain Gelly, and Mario Lucic. On mutual information maximization for representation learning. *arXiv preprint arXiv:1907.13625*, 2019.

[37] Martin Arjovsky, Léon Bottou, Ishaaan Gulrajani, and David Lopez-Paz. Invariant risk minimization. *arXiv preprint arXiv:1907.02893*, 2019.

[38] Nello Cristianini, John Shawe-Taylor, Andre Elisseeff, and Jaz Kandola. On kernel-target alignment. *Advances in neural information processing systems*, 14, 2001.

[39] Corinna Cortes, Mehryar Mohri, and Afshin Rostamizadeh. Algorithms for learning kernels based on centered alignment. *The Journal of Machine Learning Research*, 13(1):795–828, 2012.

[40] Simon Kornblith, Mohammad Norouzi, Honglak Lee, and Geoffrey Hinton. Similarity of neural network representations revisited. In *International conference on machine learning*, pages 3519–3529. PMLR, 2019.

- [41] Cian Eastwood and Christopher KI Williams. A framework for the quantitative evaluation of disentangled representations. In *International conference on learning representations*, 2018.
- [42] Sungbin Shin, Yohan Jo, Sungsoo Ahn, and Namhoon Lee. A closer look at the intervention procedure of concept bottleneck models. In *International Conference on Machine Learning*, pages 31504–31520. PMLR, 2023.
- [43] Christopher M. Bishop. *Pattern Recognition and Machine Learning*. Springer, 2006. ISBN 978-0-387-31073-2.
- [44] Alec Radford, Jong Wook Kim, Chris Hallacy, Aditya Ramesh, Gabriel Goh, Sandhini Agarwal, Girish Sastry, Amanda Askell, Pamela Mishkin, Jack Clark, et al. Learning transferable visual models from natural language supervision. In *International conference on machine learning*, pages 8748–8763. PmLR, 2021.

A Complete Graphical Models

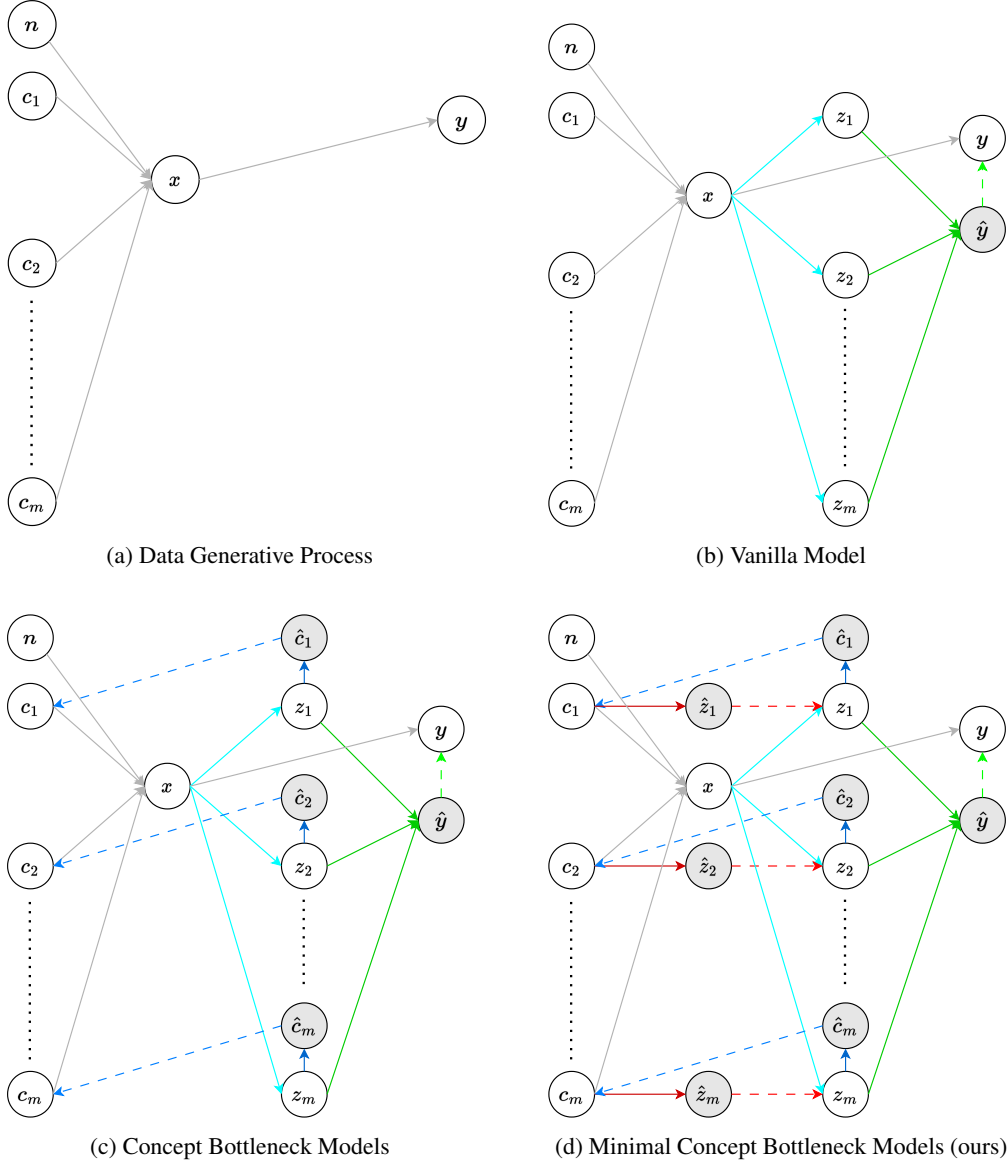


Figure 8: Graphical models of the different systems described. We consider m concepts and m -dimensional representations. Inputs x are defined by some concepts $\{c_j\}_{j=1}^m$ and nuisances n ; and targets y are defined by x (gray arrows). Vanilla models obtain the representations $\{z_j\}_{j=1}^m$ from x through the *encoder* $p_\theta(z|x)$ (cyan arrows) and solve the task \hat{y} sequentially through the *task head* $q_\phi(\hat{y}|z)$ (green arrows). Concept Bottleneck Models make a prediction \hat{c}_j of each concept c_j from one representation z_j through the *concept head* $q(\hat{c}_j|z_j)$ (blue arrows). Minimal CBMs make a prediction z_j of each representation z_j from one concept c_j through the *representation head* $q(z_j|c_j)$ (red arrows).

B Details of Derivations

B.1 Proof of Equation 1

$$I(Z; Y) = \iint p(z, y) \log \frac{p(y|z)}{p(y)} dy dz \quad (7)$$

$$= \iiint p(x, y) p_\theta(z|x) \log \frac{p(y|z)}{p(y)} dx dy dz \quad (8)$$

$$= \iiint p(x, y) p_\theta(z|x) \log \frac{p(y|z)}{p(y)} \frac{q_\phi(\hat{y}|z)}{q_\phi(\hat{y}|z)} dx dy dz \quad (9)$$

$$= \mathbb{E}_{p(x,y)} [\mathbb{E}_{p_\theta(z|x)} [\log q_\phi(\hat{y}|z)]] + E_{p_\theta(z)} [D_{KL}(p(y|z) || q_\phi(\hat{y}|z))] + H(Y) \quad (10)$$

$$\geq \mathbb{E}_{p(x,y)} [\mathbb{E}_{p_\theta(z|x)} [\log q_\phi(\hat{y}|z)]] + H(Y) \quad (11)$$

Thus, since $H(Y)$ is independent of θ and ϕ , we have that:

$$\max_Z I(Z; Y) = \max_{\theta, \phi} \mathbb{E}_{p(x,y)} [\mathbb{E}_{p_\theta(z|x)} [\log q_\phi(\hat{y}|z)]] \quad (12)$$

B.2 Proof of Equation 2

$$I(Z_j; C_j) = \iint p(z_j, c_j) \log \frac{p(c_j|z_j)}{p(c_j)} dc_j dz_j \quad (13)$$

$$= \iiint p(x, c_j) p_\theta(z_j|x) \log \frac{p(c_j|z_j)}{p(c_j)} dx dc_j dz_j \quad (14)$$

$$= \iiint p(x, c_j) p_\theta(z_j|x) \log \frac{p(c_j|z_j)}{p(c_j)} \frac{q(\hat{c}_j|z_j)}{q(\hat{c}_j|z_j)} dx dc_j dz_j \quad (15)$$

$$\geq E_{p(x,c_j)} [\mathbb{E}_{p_\theta(z_j|x)} [\log q(\hat{c}_j|z_j)]] + E_{p_\theta(z_j)} [D_{KL}(p(c_j|z_j) || q(\hat{c}_j|z_j))] + H(C_j) \quad (16)$$

$$\geq E_{p(x,c_j)} [\mathbb{E}_{p_\theta(z_j|x)} [\log q(\hat{c}_j|z_j)]] + H(C_j) \quad (17)$$

Given the fact that $H(C_j)$ is constant, we have that:

$$\max_{Z_j} I(Z_j; C_j) = \max_{\theta} E_{p(x,c_j)} [\mathbb{E}_{p_\theta(z_j|x)} [\log q(\hat{c}_j|z_j)]] \quad (18)$$

B.3 Proof of Equation 4

$$I(Z_j; X|C_j) = \iiint p(x, c_j) p_\theta(z_j|x) \log \frac{p(z_j|x)}{p(z_j|c_j)} dx dc_j dz_j \quad (19)$$

$$= \iiint p(x, c_j) p_\theta(z_j|x) \log \frac{p(z_j|x)}{p(z_j|c_j)} \frac{q(\hat{z}_j|c_j)}{q(\hat{z}_j|c_j)} dx dc_j dz_j \quad (20)$$

$$= \mathbb{E}_{p(x,c_j)} [D_{KL}(p_\theta(z_j|x) || q(\hat{z}_j|c_j))] - E_{p(c_j)} [D_{KL}(p(z_j|c_j) || q(\hat{z}_j|c_j))] \quad (21)$$

$$\leq \mathbb{E}_{p(x,c_j)} [D_{KL}(p_\theta(z_j|x) || q(\hat{z}_j|c_j))] \quad (22)$$

Thus, we have that:

$$\min_{Z_j} I(Z_j; X|C_j) = \min_{\theta} E_{p(x,c_j)} [D_{KL}(p_\theta(z_j|x) || q(\hat{z}_j|c_j))] \quad (23)$$

B.4 KL Divergence between two Gaussian Distributions

We are given the conditional distributions:

$$\begin{aligned} p_\theta(z_j|x) &= \mathcal{N}(f_\theta(x)_j, \sigma_x^2 I), \\ q_\phi(\hat{z}_j|c_j) &= \mathcal{N}(g_\phi^z(c_j), \sigma_{\hat{z}}^2 I), \end{aligned}$$

and aim to minimize the expected KL divergence:

$$\min_{\theta, \phi} \mathbb{E}_{p(x, c_j)} [D_{\text{KL}}(p_\theta(z_j|x) \| q_\phi(\hat{z}_j|c_j))].$$

The KL divergence between two multivariate Gaussians with diagonal covariances is given by:

$$D_{\text{KL}}(\mathcal{N}(\mu_p, \Sigma_p) \| \mathcal{N}(\mu_q, \Sigma_q)) = \frac{1}{2} \left[\text{tr}(\Sigma_q^{-1} \Sigma_p) + (\mu_q - \mu_p)^\top \Sigma_q^{-1} (\mu_q - \mu_p) - d + \log \frac{\det \Sigma_q}{\det \Sigma_p} \right].$$

Applying this to our case:

- $\mu_p = f_\theta(x)_j$, $\mu_q = g_\phi^z(c_j)$,
- $\Sigma_p = \sigma_x^2 I$, $\Sigma_q = \sigma_{\hat{z}}^2 I$,
- d is the dimension of z_j .

Plugging in, we obtain:

$$D_{\text{KL}} = \frac{1}{2} \left[\frac{d\sigma_x^2}{\sigma_{\hat{z}}^2} + \frac{1}{\sigma_{\hat{z}}^2} \|f_\theta(x)_j - g_\phi^z(c_j)\|^2 - d + d \log \left(\frac{\sigma_{\hat{z}}^2}{\sigma_x^2} \right) \right].$$

Note that all terms except the squared distance are constant with respect to θ and ϕ . Therefore:

$$\mathbb{E}_{p(x, c_j)} [D_{\text{KL}}(p_\theta(z_j|x) \| q_\phi(\hat{z}_j|c_j))] = \frac{1}{2\sigma_{\hat{z}}^2} \mathbb{E}_{p(x, c_j)} [\|f_\theta(x)_j - g_\phi^z(c_j)\|^2] + \text{const.}$$

Conclusion: Minimizing the expected KL divergence

$$\min_{\theta, \phi} \mathbb{E}_{p(x, c_j)} [D_{\text{KL}}(p_\theta(z_j|x) \| q_\phi(\hat{z}_j|c_j))]$$

is equivalent (up to a scaling factor) to minimizing the expected mean squared error:

$$\min_{\theta, \phi} \mathbb{E}_{p(x, c_j)} [\|f_\theta(x)_j - g_\phi^z(c_j)\|^2].$$

C Training Algorithm of MCBMs

Algorithm 1 Training Algorithm for MCBMs

Input: Dataset $\mathcal{D} = \{\mathbf{x}^{(k)}, \mathbf{y}^{(k)}, \mathbf{c}^{(k)}\}_{k=1}^N$, latent norm λ , learning rate η , batch size B
Output: Parameters θ (encoder), ϕ (class-head, task-heads, representation-heads)

- 1: Initialize parameters θ, ϕ and representations heads:
- 2: **for all** $j = 1, \dots, n$ **do**
- 3: **if** c_j is binary **then**
- 4: $g_j^z \leftarrow \lambda$ if $c_j = 1$ else $-\lambda$
- 5: **else if** c_j is multiclass **then**
- 6: $g_j^z \leftarrow \lambda \cdot \text{one_hot}(c_j)$
- 7: **else**
- 8: $g_j^z \leftarrow \lambda \cdot c_j$
- 9: **end if**
- 10: **end for**
- 11: **while** not converged **do**
- 12: Sample a mini-batch $\{\mathbf{x}^{(k)}, \mathbf{y}^{(k)}, \mathbf{c}^{(k)}\}_{k=1}^B \sim \mathcal{D}$
- 13: **for all** $\mathbf{x}^{(k)}, \mathbf{y}^{(k)}, \mathbf{c}^{(k)}$ in batch **do**
- 14: Encode: Compute $\mu_\theta^{(k)} \leftarrow f_\theta(\mathbf{x}^{(k)})$
- 15: Sample noise $\epsilon \sim \mathcal{N}(0, I)$ ▷ Reparameterization trick with only one sample
- 16: Reparameterize: $\mathbf{z}^{(k)} \leftarrow \mu_\theta^{(k)} + \sigma_x \odot \epsilon$
- 17: Task prediction: $\hat{\mathbf{y}}^{(k)} \leftarrow g_\phi^y(\mathbf{z}^{(k)})$ ▷ Similar to VMs
- 18: Task loss: $\mathcal{L}_y^{(k)} \leftarrow \|\mathbf{y}^{(k)} - \hat{\mathbf{y}}^{(k)}\|^2$ if \mathbf{y} is continuous else $\text{CE}(\mathbf{y}^{(k)}, \hat{\mathbf{y}}^{(k)})$
- 19: **for all** $j = 1, \dots, n$ **do**
- 20: Concept j prediction: $\hat{c}_j^{(k)} \leftarrow g_{\phi,j}^c(\mathbf{z}_j^{(k)})$ ▷ Similar to CBMs
- 21: Concept j loss: $\mathcal{L}_{c,j}^{(k)} \leftarrow \|\mathbf{c}_j^{(k)} - \hat{c}_j^{(k)}\|^2$ if c_j is continuous else $\text{CE}(\mathbf{c}_j^{(k)}, \hat{c}_j^{(k)})$
- 22: Representation j prediction: $\hat{z}_j^{(k)} \leftarrow g_j^z(\mathbf{c}_j^{(k)})$ ▷ Novelty in MCBMs
- 23: Representation j loss: $\mathcal{L}_{z,j}^{(k)} \leftarrow \|\mathbf{z}_j^{(k)} - \hat{z}_j^{(k)}\|^2$
- 24: **end for**
- 25: Total loss: $\mathcal{L}^{(k)} \leftarrow \mathcal{L}_y^{(k)} + \beta \sum_{j=1}^n \mathcal{L}_{c,j}^{(k)} + \gamma \sum_{j=1}^n \mathcal{L}_{z,j}^{(k)}$
- 26: **end for**
- 27: Update θ, ϕ using gradient descent:

$$\theta \leftarrow \theta - \eta \nabla_\theta \left(\frac{1}{B} \sum_{k=1}^B \mathcal{L}^{(k)} \right), \quad \phi \leftarrow \phi - \eta \nabla_\phi \left(\frac{1}{B} \sum_{k=1}^B \mathcal{L}^{(k)} \right)$$
- 28: **end while**

D Hard Concept Bottleneck Models

As discussed in Section 3, one of the most successful approaches to mitigating information leakage is the family of *Hard Concept Bottleneck Models* (HCBMs) [18]. Unlike MCBMs, which enforce an Information Bottleneck (IB) directly at the representation level z , HCBMs operate by pruning the information contained in z before producing the task prediction \hat{y} . In doing so, they encourage \hat{y} to depend solely on c , thereby yielding interventions that are more reliable in practice. This approach differs fundamentally from MCBMs: whereas Equation 4 in MCBMs minimizes over Z_j , thereby removing nuisances directly from the representation z_j , HCBMs optimize at the prediction level, focusing on \hat{Y} . Formally, they are trained to minimize:

$$\min_{\hat{Y}} I(\hat{Y}; X|C) = \min_{\theta, \phi} \mathbb{E}_{p(x, c_j)} [D_{KL}(p_{\theta, \phi}(\hat{y}|x) || p(\hat{y}|c))] \quad (24)$$

That is, the optimization is performed directly over the predictions \hat{y} . To implement this, it defines:

$$p_{\theta, \phi}(\hat{y}|x) = \iiint q_{\phi}(\hat{y}|\hat{c}^b) p(\hat{c}^b|\hat{c}) q(\hat{c}|z) p_{\theta}(z|x) d\hat{c}^b d\hat{c} dz \quad (25)$$

where $q_{\phi}(\hat{y}|\hat{c}^b)$ denotes the new *task head*, $q(\hat{c}|z)$ the *concept head*, and $p_{\theta}(z|x)$ the encoder, as defined in Section 2. The distribution

$$p(\hat{c}_j^b|\hat{c}_j) = \delta(\hat{c}_j^b - \Theta(\hat{c}_j - 0.5)) \quad (26)$$

referred to as the *binarizing head*, applies the Heaviside step function Θ to produce a binary version $\hat{c}_j^b \in \{0, 1\}$ of \hat{c}_j . In this way, HCBMs enforce an ad-hoc Information Bottleneck by predicting \hat{y} from binarized concept representations. This process is schematized in Figure 9.

How are Interventions Performed in HCBMs? Because HCBMs introduce a bottleneck immediately before predicting \hat{y} , the intervention process is more straightforward than in standard CBMs. More specifically, interventions are carried out according to:

$$p(\hat{y}|c_j = \alpha, x) = \iint q_{\phi}(\hat{y}|\hat{c}_j^b, \hat{c}_{\setminus j}^b) p(\hat{c}_j^b|c_j = \alpha) p_{\theta}(\hat{c}_{\setminus j}^b|x) d\hat{c}_j^b d\hat{c}_{\setminus j}^b \quad (27)$$

Here, $p(\hat{c}_j^b|c_j = \alpha)$ is approximated as $\delta(\hat{c}_j^b - \alpha)$, while the other distributions are available in closed form. Although this procedure provides stronger guarantees than the intervention mechanisms in standard CBMs, two main issues remain:

- (i) The optimization is performed over the predictions \hat{y} instead of the representation z . As a result, the representations themselves are not necessarily interpretable, as evidenced in Figure 4, which limits one of the core motivations for adopting CBMs in the first place.
- (ii) HCBMs still require binarizing multiclass concepts, which introduces theoretical limitations and practical drawbacks, as further discussed in Section 5.

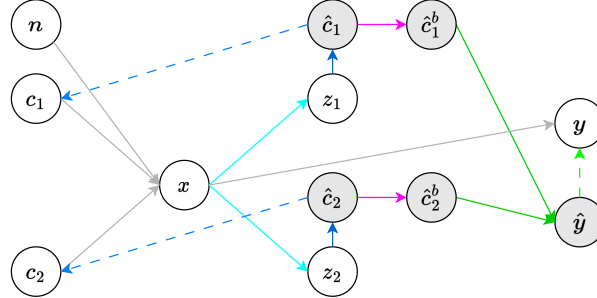


Figure 9: Graphical models of HCBMs with two concepts and two-dimensional representations. Hard Concept Bottleneck Models obtain a binarized version \hat{c}_j^b of each predicted concept \hat{c}_j through the *binarizing head* $p(\hat{c}_j^b|\hat{c}_j)$ (fuchsia arrows). Unlike the models in Figure 2, HCBMs predict the task output \hat{y} from the binarized concepts \hat{c}_j^b using the new *task head* $q_{\phi}(\hat{y}|z)$ (green arrows).

E Experiments Details

E.1 Hyperparameters for Section 4

Table 7: Hyperparameters for Section 4. For all datasets, the concept head g_ϕ^c is implemented as the identity function in CBMs, and as a multilayer perceptron (MLP) with three hidden layers in MCBMs. We emphasize that CBMs are, by design, restricted to use invertible g_ϕ^c to enable intervention procedures.

	MPI3D	Shapes3D	CIFAR-10	CUB
f_θ architecture	ResNet20	ResNet20	2 conv. layers	InceptionV3
f_θ pretraining	None	None	None	ImageNet
g_ϕ^y hidden layers	64	64	64	256
low γ	1	1	0.1	0.05
medium γ	3	3	0.3	0.1
high γ	5	5	0.5	0.3
number of epochs	50	50	200	250
batch size	128	128	128	128
optimizer	SGD	SGD	Adam	SGD
learning rate	6×10^{-3}	6×10^{-3}	1×10^{-4}	2×10^{-2}
momentum	0.9	0.9	0.	0.9
weight decay	4×10^{-5}	4×10^{-5}	4×10^{-5}	4×10^{-5}
scheduler	Step	Step	Step	Step
step size (epochs)	20	20	80	100
scheduler γ	0.1	0.1	0.1	0.1

E.2 Datasets

MPI3D This is a synthetic dataset with controlled variation across seven generative factors: *object shape*, *object color*, *object size*, *camera height*, *background color*, *horizontal axis*, and *vertical axis*. In our setup, \mathbf{y} corresponds to the *object shape*, \mathbf{n}_y to the *horizontal axis*, $\mathbf{n}_{\bar{y}}$ to the *vertical axis*, and \mathbf{c} to the remaining generative factors. To ensure consistency in the mapping between concepts and task nuisances and the target, we filter the dataset such that any combination of elements in $\{\mathbf{c}, \mathbf{n}_y\}$ corresponds to a unique value of \mathbf{y} . All invalid combinations are removed accordingly.

Shapes3D This synthetic dataset consists of 3D-rendered objects placed in a room, with variation across six known generative factors: *floor color*, *wall color*, *object color*, *scale*, *shape*, and *orientation*. In our setup, \mathbf{y} corresponds to the *shape*, \mathbf{n}_y includes *floor color* and *wall color*, $\mathbf{n}_{\bar{y}}$ corresponds to *orientation*, and \mathbf{c} comprises the remaining factors. We follow the same filtering strategy as in MPI3D to construct this configuration: we retain only those samples for which each combination of $\{\mathbf{c}, \mathbf{n}_y\}$ uniquely determines \mathbf{y} , removing all invalid configurations.

CIFAR-10 CIFAR-10 is a widely used image classification benchmark consisting of 60,000 natural images of size 32×32 , divided into 10 classes (e.g., airplanes, automobiles, birds, cats, etc.). The dataset is split into 50,000 training and 10,000 test images, with balanced class distributions. To reduce the need for manual concept annotations, the concepts are synthetically derived following the methodology of [23]. A total of 143 attributes are extracted using GPT-3 [33]; 64 form the concept set \mathbf{c} , while the rest define the nuisance set \mathbf{n}_y . Binary values are obtained with the CLIP model [44] by comparing the similarity of each image to the embedding of an attribute and to its negative counterpart.

CUB The Caltech-UCSD Birds (CUB) dataset contains 11,788 images of 200 bird species, annotated with part locations, bounding boxes, and 312 binary attributes. Following the approach of Koh et al. [9], we retain only the attributes that are present in at least 10 species (based on majority voting), resulting in a filtered set of 112 attributes. These attributes are grouped into 27 semantic clusters, where each group is defined by a common prefix in the attribute names. In our setup, the task variable \mathbf{y} is to classify the bird species. The concept set \mathbf{c} consists of the attributes belonging to 12 randomly selected groups (per run), while the nuisance set \mathbf{n}_y includes the attributes from the remaining 20 groups. Since most attributes exhibit some correlation with the classification task, we set $\mathbf{n}_{\bar{y}}$ to the empty set.